Journal of Translational Medicine

RESEARCH

Open Access

Transcriptomics of tissue exosomes to investigate miR-195-5p's amelioration of endometrial fibrosis via the YAP-Smad7 pathway: an animal study

Jia-ming Chen[1†], Qiao-yi Huang[1†], Wei-hong Chen[1], Jin-xiang Wu[2], Ling-tao Zheng[1], Hui-jie You[1], Yan-chuan Shi[3,4], Shu Lin[3,5*] and Qi-rong Shi[1*]

Abstract

Background A significant research gap exists regarding the role of tissue exosomes in intrauterine adhesions (IUAs). This study aims to investigate the involvement of miR-195-5p and its regulatory network in IUAs through the analysis of tissue exosomes.

Methods Exosomes from rat uterine tissue with intrauterine adhesions were analyzed via transcriptomics to identify downstream target genes of miR-195-5p, cross-referencing with the human endometrial transcriptomics database GSE224093. Dual luciferase labeling confirmed miRNA-target gene interactions. The therapeutic efficacy of a miR-195-5p agonist was assessed in vivo through HE staining, Masson staining, and mating tests. The mechanisms underlying extracellular matrix (ECM) deposition and myofibroblast transdifferentiation in endometrial fibrosis were investigated both in vitro and in vivo using RT-PCR, Western Blot, immunofluorescence, and immunohistochemistry. Migration ability of endometrial stromal cells was evaluated using CCK8, scratch tests, and Transwell assays. Finally, the clinical potential of miR-195-5p was compared with autologous adipose-derived mesenchymal stem cells.

Results The expression of miR-195-5p in uterine tissue exosomes from intrauterine adhesions was found to be decreased. Treatment with a miR-195-5p agonist resulted in improved endometrial health, reduced fibrosis, increased glandular density, and enhanced birth rates in rats. Both in vivo and in vitro experiments confirmed that miR-195-5p decreased ECM deposition, reduced myofibroblast transdifferentiation, and inhibited the migration of endometrial stromal cells. This was achieved through the downregulation of YAP expression in the Hippo pathway and the upregulation of Smad7. Notably, the therapeutic efficacy of miR-195-5p agonists was comparable to that of stem cell therapy, offering promising avenues for clinical application.

Conclusions Differential expression of miR-195-5p in tissue exosomes can reduce ECM deposition and myofibroblast transdifferentiation, improving endometrial fibrosis by regulating the YAP-Smad7 pathway in the Hippo signaling cascade.

†Jia-ming Chen and Qiao-yi Huang contributed equally to this article.

*Correspondence:
Shu Lin
shulin1956@126.com
Qi-rong Shi
wsqy214@163.com
Full list of author information is available at the end of the article

Keywords Tissue exosomes, miR-195-5p, Intrauterine adhesion, Myofibroblast transdifferentiation, YAP–Smad7, Hippo pathway

Background

Intrauterine adhesions (IUAs) are complications arising from damage to the basal layer of the endometrium, often caused by mechanical trauma, infection, or other factors [1]. Common symptoms include irregular menstruation, and more severe consequences can lead to infertility. In some instances, extensive uterine wall adhesions can prevent embryo implantation and fetal development, even if the fallopian tubes are unobstructed [2]. Various strategies have been developed to prevent and treat, such as transcervical resection of adhesions [3], intrauterine balloon [4], and intrauterine stents [5–7].

Our previous studies have demonstrated the efficacy of autologous adipose-derived mesenchymal stem cells in treating IUAs [8]. Meta-analyses have shown that both autologous and allogeneic stem cell treatments increase endometrial thickness, with autologous stem cell therapy yielding a higher pregnancy rate [9]. However, challenges such as difficulty and cost of autologous stem cell extraction and potential immune rejection with allogeneic stem cells have shifted interest towards exosomes [10].Exosomes are nanoscale structures containing proteins, genetic molecules, and metabolites, gaining attention as therapeutic and biomarker candidates, especially in cancer diagnosis [11, 12]. Exosomes regulate microRNAs (miRNAs) and downstream target genes; abnormal miRNA expression or function is a crucial step in the pathogenesis of many fibrotic diseases [13].

Research on the role of miRNAs in IUAs is limited. Recent studies have shown significant differences in the expression of 56 miRNAs between IUA patients and those with normal endometrium. Among these, miRNA-326 and miRNA-29b have been reported to reduce endometrial fibrosis in IUAs by inhibiting the Sp1-TGF-β1/Smad-CTGF axis [13, 14], while upregulation of miRNA-214 may be applicable in treating endometrial fibrosis [15]. Conversely, miRNA-1291 promotes endometrial fibrosis via the RhoA/ROCK1 signaling pathway, attenuated by its antagonist [16]. Thus, regulating relevant miRNAs can potentially treat endometrial fibrosis.

The cellular and molecular mechanisms underlying IUAs remain unclear. Research indicates that two key pathophysiological changes contribute to uterine adhesion fibrosis: the epithelial-mesenchymal transition (EMT) of endometrial epithelial cells [17, 18] the transdifferentiation of endometrial stromal cells into myofibroblasts. [19, 20]. Activated myofibroblasts produce extracellular matrix (ECM), leading to irreversible structural changes in the endometrial matrix. Besides epithelial cells and fibroblasts, immune system cells like macrophages and endothelial cells [21, 22], as well as smooth muscle cells involved in blood vessel formation, play roles in this process.

Myofibroblast transdifferentiation is linked to various fibrotic diseases, including renal fibrosis [23], age-related tissue fibrosis [24] and hypertrophic scars [25]. After endometrial injury, connective tissue growth factor (CTGF) activates fibroblasts via TGF-β, resulting in excessive collagen deposition and inhibiting normal regeneration of endometrial stromal cells [26, 27]. Additionally, studies have highlighted elevated NF-κB expression in IUA endometrium, promoting endometrial inflammation [28]. and damaged endometrial cells stimulating the Th2 immune response, further fostering fibrosis [29]. These pathways provide insights into potential new therapies for IUAs aimed at promoting endometrial regeneration.

Recent studies emphasize the significant role of the Hippo pathway and its transcriptional effectors, TAZ and YAP, in tissue fibrosis and myofibroblast activation [30]. The Hippo/TAZ signaling pathway regulates myofibroblast differentiation by promoting the expression of α-smooth muscle actin (α-SMA) and CTGF, and influences stem cell growth and differentiation [31, 32]. Brewer et al. found that scar repair is closely linked to Hippo-YAP signaling, suggesting potential for scar-free healing by modulating Hippo pathway activity and inhibiting myofibroblast differentiation [33]. Shen et al. indicated that Hippo downstream effectors YAP and TAZ enhance SMAD2 stability, promoting the fibrotic response. Inhibiting YAP/TAZ activity in obese mice significantly alleviates adipose tissue fibrosis and improves metabolic homeostasis [34].

The Hippo/TAZ pathway, known for its role in contact inhibition and organ size control, is activated during cell differentiation and regulates cell proliferation and fibrosis. TAZ, a crucial sensor of the Hippo pathway, translocates from the cytoplasm to the nucleus upon activation, binding to transcription factors like TEAD and Smads to regulate α-SMA and CTGF expression [31, 32, 35]. Previous research has indicated that the Hippo pathway promotes mesenchymal-epithelial transition (MET) and reverses EMT, alleviating liver fibrosis [36]. Additionally, the Hippo signaling pathway influences endometrial

stromal cell activity by regulating CTGF transcription, impacting the occurrence and progression of endometriosis [37]. Zhang et al. found that platelets combined with menstrual blood-derived stem cells could alleviate endometrial fibrosis through the CTGF pathway within the Hippo pathway, suggesting its relevance to IUAs and fibrosis [38]. Exploring the Hippo pathway's role in endometrial fibrosis aids in understanding the mechanisms underlying IUAs and identifies potential therapeutic targets.

This study aimed to explore the role of differential miR-195-5p and its regulatory network in uterine adherent tissue exosomes in IUAs. We designed animal experiments to assess miR-195-5p expression differences by exosome sequencing in normal and IUA groups, identifying YAP-Smad7 in the Hippo pathway as a downstream target gene of miR-195-5p.

Methods

Experimental animals

Six-week-old female Sprague–Dawley (SD) rats were purchased from the Experimental Animal Center of the Second Affiliated Hospital of Fujian Medical University. All animal experiments were approved by the Animal Care Committee of the Second Affiliated Hospital of Fujian Medical University and were conducted in accordance with the "Guidelines for Experimental Animal Care and Use of the National Institutes of Health" (No. 2023-179). SD rats were housed in standard cages at 22 °C on a light–dark cycle for 12 h and had unrestricted access to food and water.

Separation of exosomes from tissue

Differential ultracentrifugation was used to isolate the exosomes. Briefly, tissues were rinsed twice with phosphate buffered saline (PBS) (Sangon Biotech, E607008). Tissue specimens were cut into approximately 1 mm^3 tissue fragments with ophthalmic scissors, placed in 50 ml centrifuge tubes, and an equal volume of 0.2% type I collagenase (Sigma, C9407) solution was added and then placed in a thermostatic incubator (ESCO, CCL-170B-8). Digestion was carried out at 37 °C for 1 h until the cell suspension was milky white and was terminated with DMEM culture medium containing 10% exosome-free serum (SBI, EXO-FBS-50A-1). The supernatant was collected by centrifugation at 2000×*g* for 15 min, transferred to a new centrifuge tube, and centrifuged at 2000×*g* at 4 °C for 30 min. Afterward, the supernatant was transferred to a new centrifuge tube and centrifuged again at 10,000×*g* for 45 min 4 °C to remove larger vesicles. The supernatant was filtered through a 0.45 μm filter membrane, and the filtrate was transferred to a new centrifuge tube and centrifuged at 100,000×*g* for 70 min at 4 °C with the ultra-high-speed rotor selected. The supernatant was removed and re-suspended with 10 mL of pre-cooled 1 × PBS. The filtrate was then centrifuged by selecting the high-speed rotor at 100,000×*g* for 70 min 4 °C. The supernatant was then removed and resuspended with 100 μL of pre-cooled 1 × PBS.

Transmission electron microscopy

The exosomes were diluted in ratio 1:2 to a volume of 10 μL. The sample was precipitated by adding 10 μL to a copper grid for 1 min and floating liquid was absorbed with filter paper. Uranium acetate (10 μL) was added dropwise to the copper mesh to precipitate for 1 min and the floating liquid was removed with filter paper. The samples were allowed to dry at room temperature. Electron microscope imaging was performed using 100 kV, and imaging results (Hitachi, HT-7700) were obtained.

Particle size analysis

A nano flow cytometer (NanoFCM, N30E) was used to determine the size distribution and concentration of the exosomes. The exosomes were diluted ratio 1:6 to a total volume of 30 μL. After passing the standard instrument performance test, the exosome sample was loaded. Attention was paid to the necessity of gradient dilution to avoid the sample blocking the injection needle. When the sample is complete, information on the particle size and concentration of exosomes detected by the instrument can be obtained.

Fluorescent labelling and nanofluid detection

Exosomes were diluted in a ratio of 1:4.5 to a total volume of 90 μL, and 30 μL of diluted exosomes were added to 20 μL of fluorescent-labeled antibodies (CD9, CD81, IgG) (BD), mixed, and incubated at 37 °C for 30 min. One milliliter of pre-cooled PBS was added followed by ultracentrifugation for 70 min at 4 °C, 110,000×*g* with the ultra-rotator selected. The supernatant was carefully removed and 1 mL of pre-cooled PBS was added, followed by ultracentrifugation at 4 °C, 110,000×*g* for 70 min with the ultra-rotator selected. The supernatant was carefully removed and resuspension with 50 μL of pre-cooled 1 × PBS was performed. After the instrument performance test with the standard was passed, the exosome sample was loaded. It should be noted that a gradient dilution is required to avoid sample blocking of the injection needle. After the sample was tested, the instrument's protein index results became available.

High-throughput sequencing and bioinformatics analysis

According to exosomal RNA concentration, the appropriate amount of RNA stock solution was diluted with NR1 clip matching diluent, diluted, and tested on the

machine. Data results were screened by the data control software Fast p (https://github.com/OpenGene/fastp) and low-quality data were filtered. The filtering criteria were as follows: (1) removal of reads containing the adapter; (2) removal of reads with n ratios > 10%; (3) removal of all A-base reads; (4) removal of low-quality reads (quality value Q' 20); and (5) removal of sequences with an effective length < 20 nt. Clean reads were finally obtained after exclusion. Comparative analyses were then performed using STAR software based on the reference genome (NCBI assembly mRatBN7.2), and the protein coding genes were quantified and annotated by feature counts. DESeq2 was used for miRNA differential expression analysis. The screening criteria for differential genes were corrected for the threshold for significant screening: p-value < 0·05 and $|\log FC| \geq 1$.

To predict the potential miRNAs binding with mRNA, the miRDB (http://www.mirdb.org/) and miRWalk (http://mirwalk.umm.uni-heidelberg.de/) databases were used to search for miR-195-5p target genes. The target genes were analyzed by the string database and Cytoscape screening for target genes; functional enrichment analysis was performed using the cluster Profiler software package in R language.

Quantitative reverse transcription polymerase chain reaction (qRT-PCR)

Total RNA from uterine tissues was extracted with Trizol reagent (BioSharp, Shanghai, China), and the purity and concentration of RNA were determined spectrophotometrically. Reverse transcription and cDNA synthesis were performed using a PrimeScript™ RT reagent Kit with gDNA Eraser (Perfect Real Time; Takara, Japan), according to the manufacturer's protocol. Afterward, qRT-PCR was performed in triplicate using specific primers to detect mRNA expression levels in uterine tissues. U6 (Rnu6-1) was used as an endogenous control for miRNAs, and β-actin was used as the internal control for mRNA. The expression was quantified by StepOne Plus real-time PCR system (Applied Biosystems, CA, USA). Real-time PCR was performed using the qPCR SYBR Green Mix (Takara, Japan). The relative expression levels of mRNA and miRNA were calculated by the $2^{-\Delta\Delta Ct}$ method. The primer sequences are shown in Table 1.

Western blotting

The uteri of the animals were lysed with radioimmunoprecipitation assay buffer (Meron Bio, China) supplemented with 1 μL/100 μL protease inhibitor and phosphatase inhibitor (Meron Bio, China) for 30 min. The supernatant was collected by centrifugation at 4 °C for 10 min at 13,000×*g*. The total protein concentration was determined by BCA kit (Meillunbio, China). Equal masses of proteins were resolved by dodecyl sulfate–polyacrylamide gel electrophoresis and blotted onto polyvinylidene fluoride membranes (Meillunbio, China). Afterward, they were blocked with the following primary antibodies in 5% skimmed dry milk: rabbit monoclonal anti-α-SMA (1:2000, Hua Bio, China), rabbit polyclonal anti-collagen I (1:1000, Proteintch, China), rabbit polyclonal anti-vimentin (1:1000, Proteintech, China), rabbit polyclonal anti-Smad7 (1:1000, Proteintech, China), and mouse monoclonal anti-YAP1 (1:5000, Proteintech, China). Rabbit anti-GAPDH polyclonal antibody

Table 1 qRT-PCR primers sequences

Gene name	Forward (5′–3′)	Reverse (5′–3′)	RT primer
miR-195-5p	CGCCTAGCAGCACAGAAAT	ATCCAGTGCAGGGTCCGAGG	GTCGTATCCAGTGCAGGGTCCGAGGTATTCGCACTGGATACGACGCCAAT
miR-196a-5p	CGCGCGTAGGTAGTTTCATGTT	ATCCAGTGCAGGGTCCGAGG	GTCGTATCCAGTGCAGGGTCCGAGGTATTCGCACTGGATACGACCCCAAC
miR-378a-5p	ACGAGATCCTCCTGACTCCAGG	ATCCAGTGCAGGGTCCGAGG	GTCGTATCCAGTGCAGGGTCCGAGGTATTCGCACTGGATACGACACACAG
miR-30b-5p	GCGCGTGTAAACATCCTACAC	ATCCAGTGCAGGGTCCGAGG	GTCGTATCCAGTGCAGGGTCCGAGGTATTCGCACTGGATACGACAGCTGA
miR-30e-5p	GCGCGTGTAAACATCCTTGAC	ATCCAGTGCAGGGTCCGAGG	GTCGTATCCAGTGCAGGGTCCGAGGTATTCGCACTGGATACGACCTTCCA
U6	CTCGCTTCGGCAGCAC	AACGCTTCACGAATTTGCGT	–
α-SMA	GGCTCTGGGCTCTGTAAGG	CTCTTGCTCTGGGCTTCATC	–
Collagen I	TCAGCTGCATACACAATGGC	TCTTTGCATAGCACGCCATC	–
Vimentin	GACCGCTTCGCCAACTACATCG	CGCAACTCCCTCATCTCCTCCTC	–
YAP	ACAGGAGACACCATCAGCCAGAG	CTTCCAGTGTGCCAAGGTCCAC	–
Smad7	CAAGAGGCTGTGTTGCTGTGAATC	TCGGGTATCTGGAGTAAGGAGGAG	–
β-actin	GCTGTGCTATGTTGCCCTAGACTTC	GGAACCGCTCATTGCCGATAGTG	–

(1:10,000, Affinity, China) was used as a control to quantify the protein expression level.

Vector construction and plasmid extraction

The 3'-UTR sequences of the rat Smad7 and YAP genes were retrieved from the NCBI database. Wild-type (WT) and mutant fragments, measuring 224 bp and 300 bp, respectively, were designed near the potential action site of the rno-miR-195-5p gene. Appropriate restriction enzyme sites and protective bases were added at both ends, and gene synthesis was performed by Beijing Genco Biotechnology. The successfully synthesized plasmid was cultured, and plasmid extraction was carried out using an endotoxin-free kit for cell transfection. The following are the primer sequences and sizes of the amplification products, with the action site indicated by a red marker (Supplementary file 1).

Luciferase reporter gene experiment

The interaction between miR-195-5p and SMAD7/YAP was confirmed using a luciferase reporter gene assay. The 3'UTR sequences of SMAD7 and YAP containing the predicted miR-195-5p binding site were cloned into the pmir-GLO vector to generate the wild-type (wt) vectors pmir-GLO-SMAD7/YAP-wt and mutant-type (mut) vectors pmir-GLO-SMAD7/YAP-mut (provided by Beijing Genco Biotechnology). The wt/mut SMAD7/YAP vectors were co-transfected into 293 cells with either miR-195-5p mimic or mimic NC using Reebok transfection reagent (Addison Biological, China). Transfected 293 cells were cultured in DMEM supplemented with 10% FBS and 1% penicillin/streptomycin at 37 °C with 5% CO_2 for 48 h. Subsequently, luciferase activity was measured using the dual luciferase assay kit (Biyuntian, China) on the luciferase assay system (MD, USA).

Establishment of animal models

First, the SD rats were found to have a normal estrous cycle; thus, 24 SD rats were randomly divided into four groups. All animals were anesthetized with 2% pentobarbital sodium at 0.2 mL/100 g. A double-blind method was used in the experiment. No grouping was known between the experimenter and the animal. Only the statistician knew the grouping at the end of the experiment, which reduced the partial blindness. (1) control group (n = 10): no treatment, only open laparotomy. (2) IUA group (n = 10): the middle and lower one-third of the Y-shaped uterus on both sides of the rats were scraped repeatedly with a curette spoon. After 7 days of modeling, 10 μL PBS was injected locally on both sides of the uterus. (3) nc agomir group (n = 10): after 7 days of modeling in SD rats, 5 nmol of nc mimics dissolved in 10 μL PBS was injected locally in the middle and lower one-third of the damaged uterus on both sides. (4) miR-195-5p group (n = 10): after 7 days of modeling in SD rats, 5 nmol of miR-195-5p was injected locally into the middle and lower one-third of the damaged uterus on both sides. After 7 days of treatment in all groups, 20 rats (n = 5, each group) were sacrificed and their uteruses were preserved for subsequent experiments. The remaining 20 were mated at a male-to-female ratio of 1:2, and their pregnancy and birth outcomes were observed.

Hematoxylin and eosin staining

Uteri were fixed in 4% paraformaldehyde for 24 h and then paraffin embedded. Slides were first deparaffinized and rehydrated and then stained with hematoxylin and eosin (H&E) (Solarbio, China). Panoramic images of the diseased uterus were observed, and the number of glands was counted to predict IUA. The number of glands and endometrial thickness were obtained using Image-Pro Plus 6.0 software, and the mean number of glands and mean endometrial thickness were calculated from three randomly selected fields of view from each slide.

Masson's trichrome staining

Masson's trichrome staining was used to detect the degree of endometrial fibrosis. The deparaffinized and rehydrated slides were incubated with Masson's trichrome staining mixture (Solarbio, China) for 5 min and then stained with phosphomolybdic acid-aniline blue solution (Solarbio, China) for 5 min. The ratio of the area of collagen fibers stained in blue to the total view was calculated.

Immunohistochemistry

After deaffinity, dehydration, and antigen extraction, the sections were immersed in 3% hydrogen peroxide to block endogenous peroxidase activity followed by blocking with goat serum for 1 h. Thereafter, the sections were incubated with rabbit monoclonal anti-α-SMA (1:200, Hua Bio, China), rabbit polyclonal anti-collagen I (1:500, Proteintch, China), rabbit polyclonal anti-vimentin (1:2500, Proteintech, China), rabbit polyclonal anti-Smad7 (1:200, Proteintech, China), and mouse monoclonal anti-YAP1 (1:200, Proteintech, China) at 4 °C overnight. The sections were incubated with the appropriate secondary antibody for 60 min at room temperature. Afterward, the sections were stained with 3,3-diaminobenzidine (DAB) at room temperature. Hematoxylin was slightly counterstained, dehydrated, and covered with glass slides. Immunoreactivity was quantified using Image-Pro Plus 6.0 software, and the mean optical density (MOD) was determined in 3–5 randomly selected fields of view per section.

Isolation, purification, and culture of primary endometrial stromal cells

The method of isolating stromal cells was similar to that described in previous studies. Whole endometrial tissue specimens were collected under aseptic conditions and immediately placed in PBS (Melenbio, China) containing streptomycin (100 mg/mL; Solario, China). The samples were sent to the laboratory within 30 min. Tissue specimens were washed several times with PBS, cut into 0.5–1 mm^3 sections, incubated in DMEM/F12 (Merenbio, China) supplemented with 0.2% collagenase I (Sigma-Aldrich China, Inc., Shanghai, China), and stirred at 37 °C for 60 min. Subsequently, the resulting suspension was successively filtered through sterile 100 μm and 40 μm nylon filters (NEST, China) to remove undigested substances and epithelial cells. After centrifugation at 150×*g* for 5 min at room temperature, the supernatant was discarded and the endometrial stromal cells were resuspended in the presence of 10% fetal bovine serum (Gibco, USA), plated in a 25 cm^2 flask, and incubated at 37 °C with 5% carbon dioxide. After 24 h, the medium was replaced to remove the unattached cells. The remaining adherent stromal cells were supplemented with fresh culture medium every 3 days until fusion. The third to sixth generations were used for subsequent experiments.

Treatment with TGF-β1

To investigate the function of TGF-β in primary embryonic stem cells (ESCs), we inoculated embryonic stem cells in 96-well plates at a density of 2×10^5 cells/well. The cells were initially incubated with TGF-β (0, 1, 5, 10, 20 ng/mL) for 24, 48, and 72 h, and then collected for cell viability assays.

Transfection

Cultured ESCs were inoculated in 96-well plates (3×10^3 cells/well) for cell proliferation analysis, inoculated in 6-well plates (2×10^5 cells/well) for qRT-PCR and Western blotting, and inoculated in 24-well plates for immunofluorescence staining. To prevent treatment, cells were incubated at a density of 30–50% overnight and then in serum-free culture medium for 24 h to synchronize the cell cycle. Subsequently, miR-195-5p was mimicked to RiboBio-designed miR-195-5p and miRNA control according to the manufacturer's protocol and transfected with transfection agents provided by RiboBio. Cell viability, RT-qPCR, Western blotting, and immunofluorescence analyses were performed at 24 h post-transfection and 48 h post-treatment with TGF-β (10 ng/mL) [Peprotech, New Jersey, US], respectively.

Cell viability assay

The effects of different concentrations of TGF-β on the activity of ESCs were detected using the CCK-8 method (Merenbio, China). ESCs were inoculated in 96-well plates. After 24 h, the intervention was performed with 0, 5, 10, and 20 ng/mL TGF-β for 24, 48, and 72 h, respectively. At the end of each time point, the viability of the ESCs was assessed by the CCK-8 method according to the manufacturer's plan; absorbance was measured at 450 nm using a microplate reader.

Immunofluorescence staining

The transfected ESCs were inoculated on 24-well plates with 8×8 mm slides, formaldehyde-fixed for 20 min, and then 0.5% Triton X-100-fixed and infiltrated. After incubation with 5% goat serum (Sorabio, China) for 30 min, the cells were incubated with specific primary antibody anti-α-SMA (1:200, Huabio, China), rabbit polyclonal anti-collagen I (1:200, Proteintch, China), rabbit polyclonal anti-vimentin (1:200, Proteintech, China), rabbit polyclonal anti-Smad7 (1:100, Proteintech, China), and mouse monoclonal anti-YAP1 (1:100, Proteintech, China). The cells were incubated at 4 °C for 14 h, and then incubated with the goat polyclonal alexa Fluor® 594 conjugated secondary antibodies and goat polyclonal alexa Fluor® 488 conjugated secondary antibodies (1:500, Huabio, China) for 30 min in the dark. Finally, the cells were incubated with anti-fluorescence quenchers containing DAPI for 15 min. Photographs were taken with an inverted fluorescence microscope (Nikon, Japan).

Wound healing assay

ESC migration was detected using wound healing assay. The transfected cells were inoculated in 6-well plates at a density of 1×10^5 cells/well. Thereafter, the center of the plate was scraped with the tip of a sterile plastic microtube. Cell movement was recorded using Image-Pro Plus 6.0 software. Each biological sample was performed in triplicate and the experiment was repeated three times independently.

Transwell assay

The transwell assay was used to detect the migratory ability of ESCs. After treatment with TGF-β for 2 days, endothelial cells were digested with trypsin and washed with PBS. Serum-free medium cultured ESCs from all groups were digested with trypsin and cultured in the upper chamber medium at a concentration of 2×10^4/100 μL. DMEM/F12 (600 μL) containing 10% FBS was injected into the lower chamber. After 24 h, the cells were fixed with 4% paraformaldehyde, stained with

0.1% crystal violet for 10 min, and washed three times with PBS. Each biological sample was performed in triplicate and the experiment was repeated three times independently.

Statistical analysis

Data were expressed as means ± standard deviation of three independent biological experiments, and graphs were generated by GraphPad Prism 9.4.0. Comparisons between two groups were made using the Student's t-test, and comparisons between multiple groups were made using one-way ANOVA, with statistically significant differences denoted as follows: *P < 0.05, **P < 0.01, ***P < 0.001, and ****P < 0.0001.

Results

Extracellular matrix deposition and myofibroblast transdifferentiation occurs in the pathogenesis of IUA

To monitor the estrous cycle of SD rats, examinations of the following were performed: complete proestrus, estrus, metestrus, and diestrus (Supplementary Fig. 1A). H&E staining showed that the surface of the uterine cavity in the control group was covered with columnar epithelium, and endometrial glands were abundant and arranged in a round or oval shape. In the model group, tissue adhesion was observed, the intima became thinner, and the number of glands decreased significantly (Supplement Fig. 1B, C). The area of fibrosis throughout the endometrium was calculated by Masson's trichrome staining 7 days after injury. The results showed a significant increase in the area of fibrosis after injury (Supplement Fig. 1E, F).

Western blot analysis showed increased protein levels of collagen I, α-SMA, and vimentin after injury in the test animals compared with controls (Supplement Fig. 1G, H). Furthermore, qRT-PCR analysis revealed increased mRNA expression of collagen I, α-SMA, and vimentin after injury (Supplementary Fig. 1I). This suggests the presence of ECM deposition and myofibroblast transdifferentiation in IUAs. (ns = not significant, *P < 0.05, **P < 0.01, ****P < 0.001).

Decreased expression of exosomal miR-195-5p and Smad7 mRNA in the IUA group

Extraction and identification of exosomes from uterine tissue

To investigate the potential role of myofibroblast transdifferentiation in IUA, we performed high-throughput sequencing of tissue exosomes from three IUA samples and four normal samples. First, uterine tissue exosomes were extracted by ultracentrifugation. Purified uterine tissue exosomes were identified using dynamic light scattering (DLS) analysis, transmission electron microscopy (TEM), and flow cytometry. DLS measurements showed that the diameters of these particles were predominantly 30–100 nm, which agrees with the previously reported size distribution of exosomes (Supplement Fig. 2A). TEM showed that uterine tissue exosomes were cup or spherical in shape similar to previously described exosomes (Supplementary Fig. 2B). Flow cytometry analysis further confirmed that these particles were exosomes, showing that exosome surface markers included CD63 and CD9 (Supplement Fig. 2C). All these data suggest that these nanoparticles are in fact exosomes. (ns = not significant, *P < 0.05, **P < 0.01, ****P < 0.001).

Decreased expression of miR-195-5p in IUA uteruses

Eleven differentially expressed candidate miRNAs were screened using $p < 0.05$ and $|\text{fold change}| \geq 2$ as the criteria; all 12 miRNAs were downregulated in IUA tissues compared to normal uterine tissues, which are shown in a cluster heat map and volcano map (Fig. 1A, B). In addition, stem-loop and tailed qRT-PCR further demonstrated that the expression of miR-195-5p, miR-378a-5p, miR-30a-5p, and miR-30b-5p was downregulated in IUA compared to normal uterus tissues (Fig. 1C). We selected miR-195-5p for further clinical study because it was verified on SD rats to be the most statistically significant and exhibited the largest difference. In clinical practice, 13 human endometrium and 13 endometrium of intrauterine adhesions were collected. The results of stem-loop qRT-PCR showed that the expression of miR-195-5p in endometrium of intrauterine adhesions decreased ($p < 0.05$, Fig. 1D) (ns = not significant, *P < 0.05, **P < 0.01, ****P < 0.001).

(See figure on next page.)

Fig. 1 MiR-195-5p and its downstream target gene Smad7 are decreased in IUA. **A**, **B** Heat map and volcano plot showing differential miRNAs in exosomes from normal and IUA groups. **C** Stem-loop RT-PCR results show significant decreases in miR-195-5p, miR-378a-5p, miR-30b-5p, and miR-30a-5p in SD rats with IUAs. **D** Differential expression of miR-195-5p in the endometrium of IUA patients. **E** Venn diagram of downstream target genes of human and rat miR-195-5p from miRDB and miRWalk databases. **F** Venn diagram showing the intersection of differential genes in the IUA transcriptome and miR-195-5p target genes. **G** Cytoscape shows the core genes of intersection genes. **H** Dual luciferase assays verify the targeting relationship between miR-195-5p and YAP, Smad7. **I**–**K** Western blot analysis of YAP and Smad7 expression in uterine adhesion tissues. (ns = not significant, *P < 0.05, **P < 0.01, ****P < 0.001)

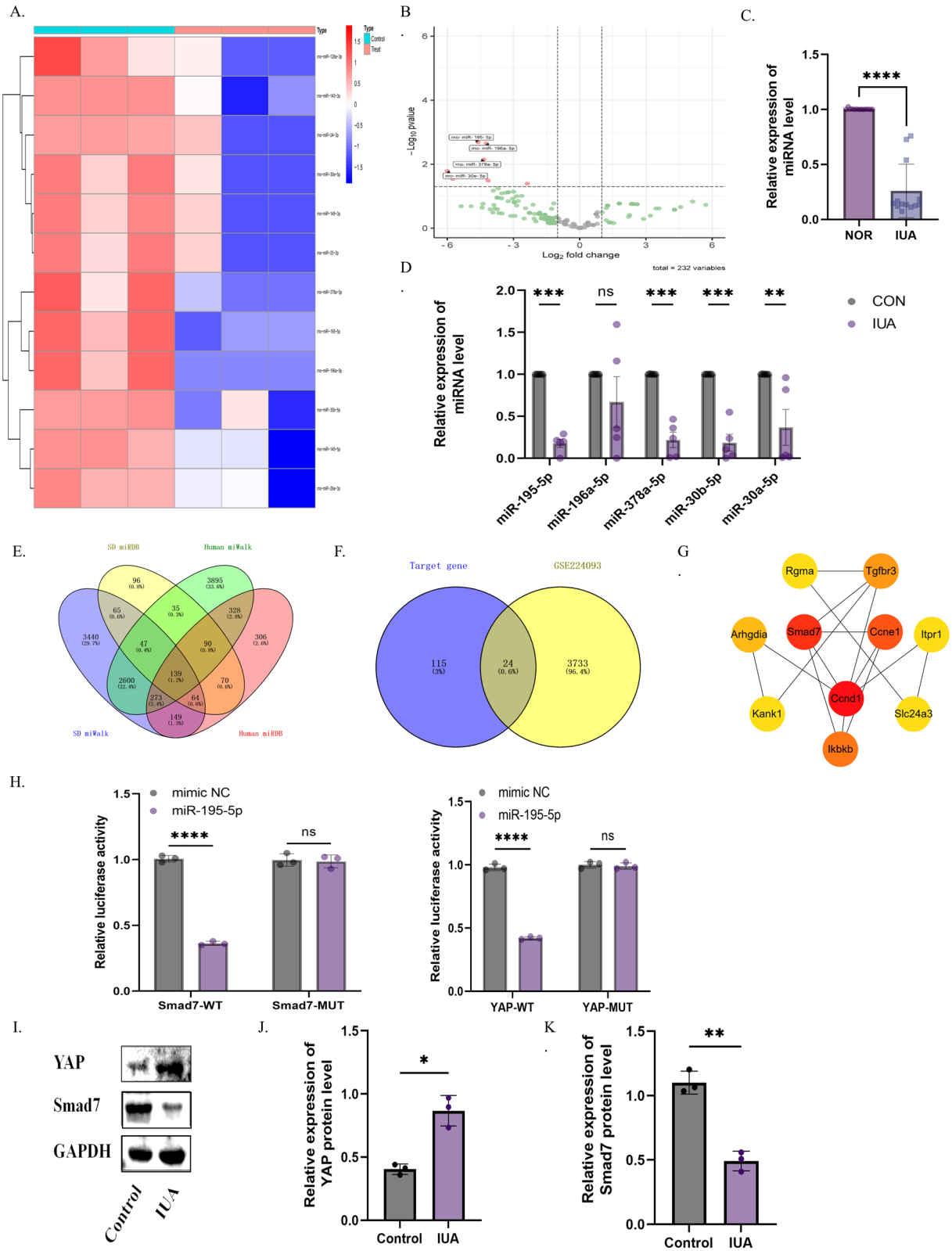

Fig. 1 (See legend on previous page.)

The expression of miR-195-5p target gene Smad7 in IUA was decreased, and the expression of YAP was increased

Using miRDB and miWalk, we screened for miR-195-5p target genes in SD rats and intersected them with human miR-195-5p target genes, resulting in a total of 139 intersecting target genes (Fig. 1E). GO and KEGG enrichment analysis revealed enrichment in pathways such as p53, Hippo, and Wnt (Supplement Fig. 3A, B). To further investigate the relationship between miR-195-5p and its downstream target genes with intrauterine adhesions, we analyzed differential genes in intrauterine adhesions from the GSE224093 transcriptomic dataset. Heatmap and volcano plot analysis identified 3757 differential genes between intrauterine adhesions and normal groups (Supplement Fig. 3C, D). Intersecting the differential genes from the transcriptome with the miR-195-5p intersecting target genes yielded 24 genes (Fig. 1F). A protein–protein interaction (PPI) network was constructed using STRING for these 24 genes (Supplement Fig. 3E), and the top ten hub genes were identified using the MCODE plugin in Cytoscape, with Smad7 ranking high (Fig. 1G). Furthermore, Smad7 was found to coexist with YAP in the Hippo pathway in the KEGG pathway analysis (Supplement Fig. 3F). (ns = not significant, *P < 0.05, **P < 0.01, ****P < 0.001).

To further investigate the targeting relationship between YAP, Smad7, and miR-195-5p, we conducted dual luciferase reporter assays for each of these components. The results demonstrated that the miR-195-5p mimic significantly inhibited the luciferase activity of YAP-WT and Smad7-WT, but had no significant effect on YAP-MUT and Smad7-MUT (Fig. 1H). Additionally, Western Blot analysis verified the expression of YAP and Smad7 in intrauterine adhesions. The results revealed increased YAP levels and decreased Smad7 levels in the intrauterine adhesion group (Fig. 1I–K) (ns = not significant, *P < 0.05, **P < 0.01, ****P < 0.001).

Based on the above findings, we observed a decrease in miR-195-5p expression in exosomes from uterine tissue of intrauterine adhesions with YAP and Smad7 identified as its downstream target genes. Furthermore, ECM deposition and myofibroblast transdifferentiation were noted during fibrosis. Hence, we proceeded to investigate the impact and mechanism of miR-195-5p agonists on ECM deposition and myofibroblast transdifferentiation in endometrial fibrosis associated with intrauterine adhesions.

Agomir-195-5p prevented endometrial fibrosis by inhibiting ECM deposition and myofibroblast transdifferentiation

Agomir-195-5p improved endometrial fibrosis

To determine the relationship between miR-195-5p and myofibroblast transdifferentiation in IUA, we overexpressed miR-195-5p in the uterus of rats by transfecting agomir-195-5p. We first determined the effect of agomir-195-5p on the expression of miR-195-5p in the uterus by qRT-PCR analysis. The expression of miR-195-5p was significantly decreased in the PBS and negative control (NC) simulated groups. In contrast, compared with the NC group, the expression of miR-195-5p in IUA rats treated with agomir-195-5p was enhanced (Fig. 2A). (ns = not significant, *P < 0.05, **P < 0.01, ****P < 0.001).

H&E staining revealed thinning of the endometrium and a decrease in the number of glands in the PBS and NC simulated treatment groups compared to the control group, while thickening of the endometrium and an increase in the number of glands in the agomir-195-5p treatment group (Fig. 2B–D). In addition, Masson tricolor staining showed an increase in fibrosis in the PBS and NC simulated treatment groups compared with the control group, and a decrease in the area of fibrosis in the agomir-195-5p treatment group (Fig. 2E, F). Additionally, mating experiments revealed that, compared to the agomir-195-5p treatment group, the PBS treatment group had a significantly reduced litter size and pregnancy rate, with an increased number of stillbirths. In contrast, the agomir-miR-195-5p treatment group exhibited improved fertility, and the pups were more robust in appearance than those in the PBS treatment group. However, a comprehensive assessment of the pups' health status was not conducted. (Fig. 2G, H). These results suggest that agomir-195-5p has a certain efficacy in the treatment of IUA, and the decrease of miR-195-5p may be a pathogenic factor for IUA (ns = not significant, *P < 0.05, **P < 0.01, ****P < 0.001).

Agomir-195-5p prevented endometrial fibrosis by inhibiting ECM deposition and myofibroblast transdifferentiation

We found that these histological changes were related to ECM deposition and myofibroblast transdifferentiation. As shown in Fig. 3A–C, qRT-PCR analysis showed that α-SMA, Collagen I, and vimentin-related indexes of myofibroblasts increased after injury in the PBS treatment group. Western blot and immunohistochemical analysis showed that compared with the control group, the levels of type I collagen, α-SMA and vimentin were increased after injury. In contrast, mRNA and protein levels after treatment with miR-195-5p agonist showed improvements in ECM deposition and related indexes of myoblast transdifferentiation (Fig. 3D–F). Thus, agomir-195-5p prevents excessive ECM deposition and myofibroblast transdifferentiation after endometrial injury (ns = not significant, *P < 0.05, **P < 0.01, ****P < 0.001).

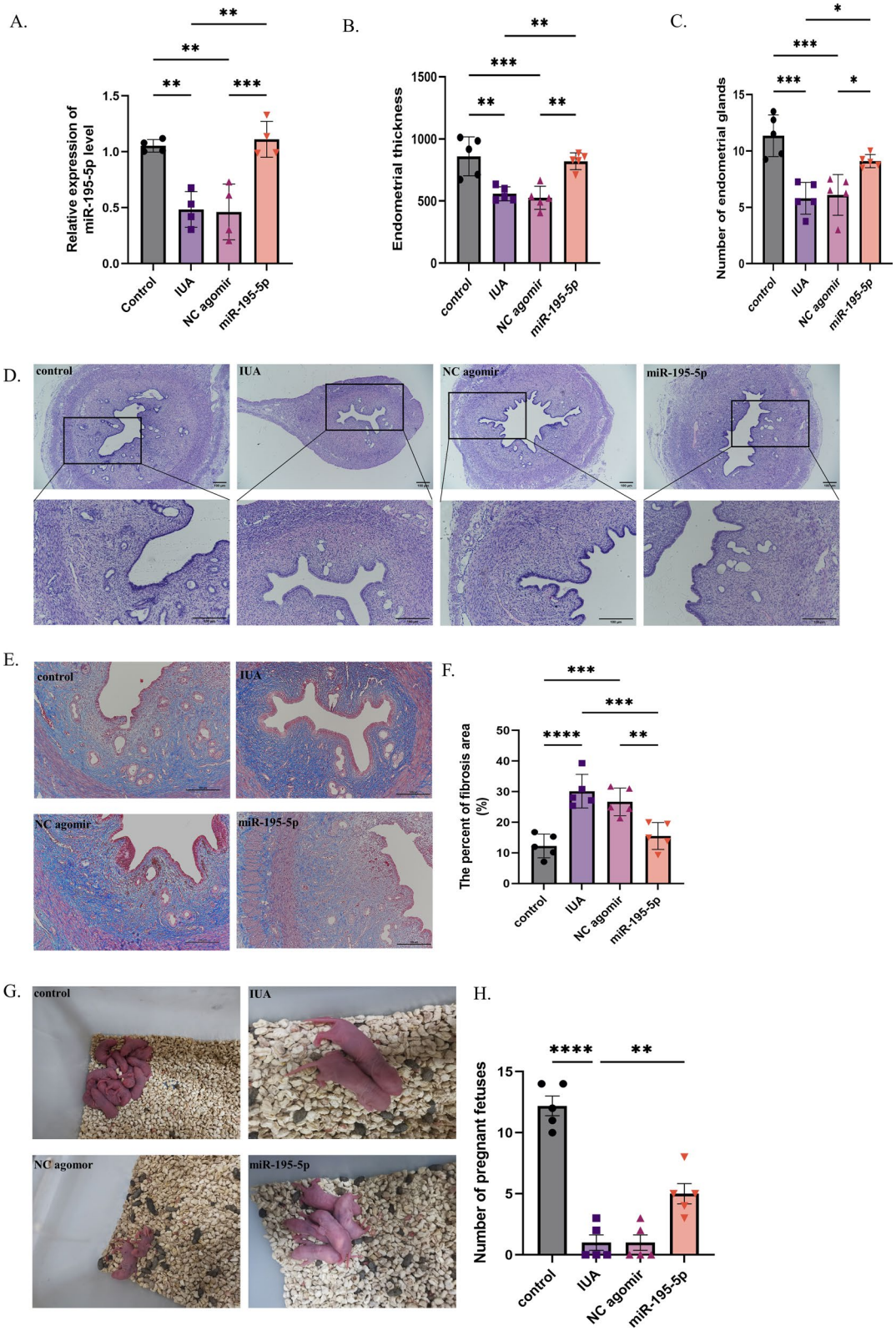

Fig. 2 Agomir-195-5p improves endometrial fibrosis and fertility. **A** RT-PCR results showing increased miR-195-5p expression in uterine tissue after agomir-195-5p treatment. **B**–**D** H&E staining of uterine morphology, with statistical analysis of endometrial thickness and gland number. **E**, **F** Assessment of fibrotic area in the endometrium using Image Pro Plus 6.0 and Masson staining. **G**, **H** Fertility experiment results. (ns = not significant, *P < 0.05, **P < 0.01, ****P < 0.001)

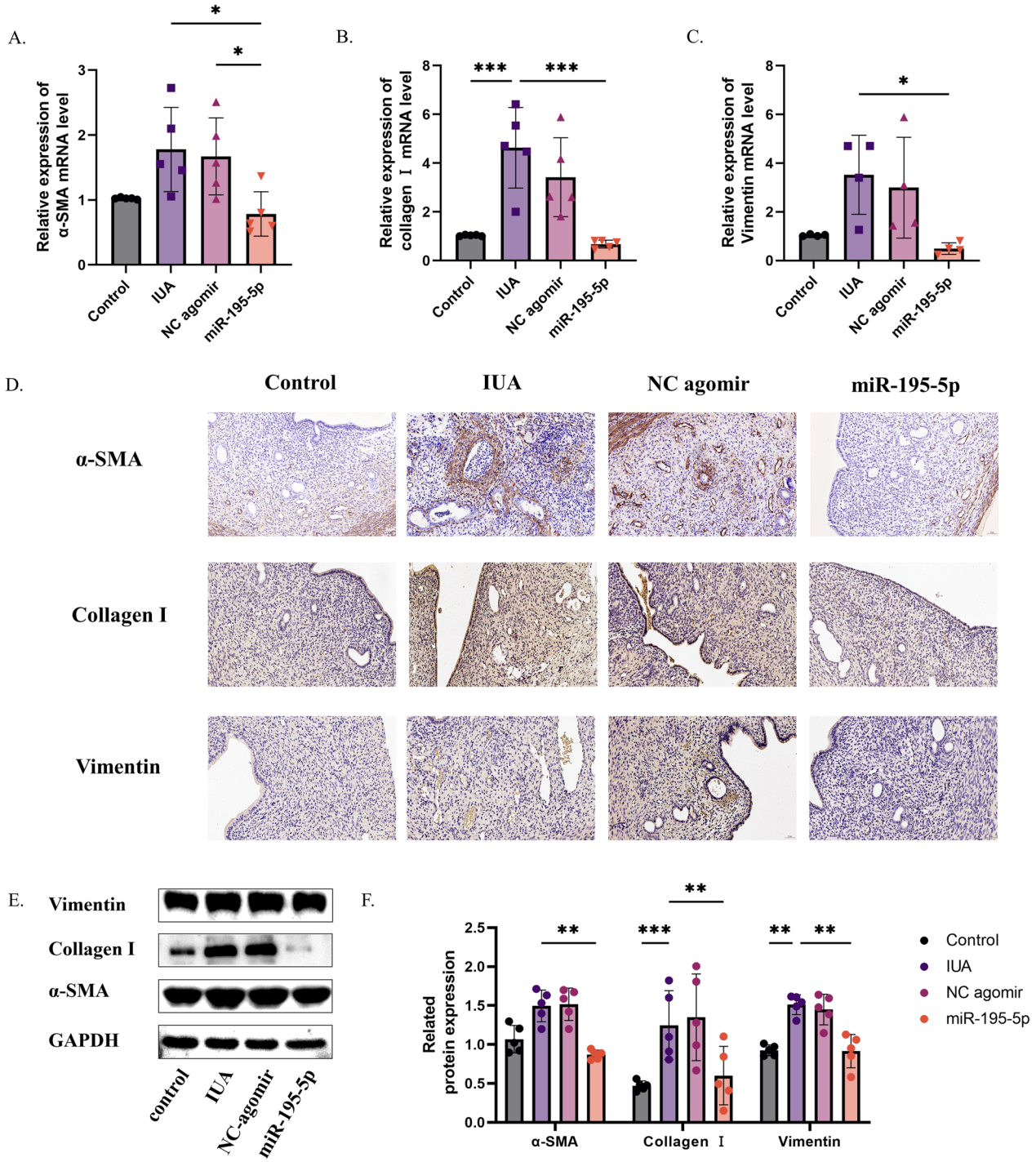

Fig. 3 Agomir-195-5p improves ECM deposition and myofibroblast transdifferentiation. **A**–**C** RT-PCR results showing changes in ECM deposition and myofibroblast transdifferentiation markers after miR-195-5p treatment. **D** Immunohistochemistry results for ECM deposition and myofibroblast transdifferentiation markers after miR-195-5p treatment. **E**, **F** Western blot results for ECM deposition and myofibroblast transdifferentiation markers after miR-195-5p treatment. (ns = not significant, *P < 0.05, **P < 0.01, ****P < 0.001)

Agomir-195-5p regulated endometrial fibrosis by inhibiting the YAP–Smad7 pathway

Bioinformatics analysis showed that Smad7 and YAP were potential targets of miR-195-5p. By qRT-PCR, immunohistochemistry, and Western blot analysis, the decrease of miR-195-5p in fibrotic endothelial tissues

was associated with the activation of YAP-Smad7 signaling. This was confirmed by increased expression of YAP mRNA and protein in fibrotic endothelium and significantly down-regulated expression of Smad7. In contrast, transfection of agomir-195-5p significantly inhibited the expression of YAP and increased the expression of Smad7 in uterine tissue after the establishment of IUA models. Thus, agomir-195-5p may inhibit endometrial fibrosis by blocking the YAP-Smad7 pathway (Fig. 4A–H) (ns = not significant, *P < 0.05, **P < 0.01, ****P < 0.001).

MiR-195-5p mimics inhibited TGF-β-induced endometrial stromal cell migration and myofibroblast transdifferentiation

Morphological observation and identification of ESCs

To further explore the reasons for the differential expression of tissue exosomal miR-195-5p and the mechanism of myofibroblast transdifferentiation, we extracted primary endometrial stromal cells from SD rats. ESCs could grow adherently at 24 h after sowing. Subsequently, 1–3 generations were observed under the microscope. The cells were fibrillar and most of the ESCs formed tightly parallel arrays (Supplement Fig. 4A). Immunofluorescence staining showed that ESCs were positive for the

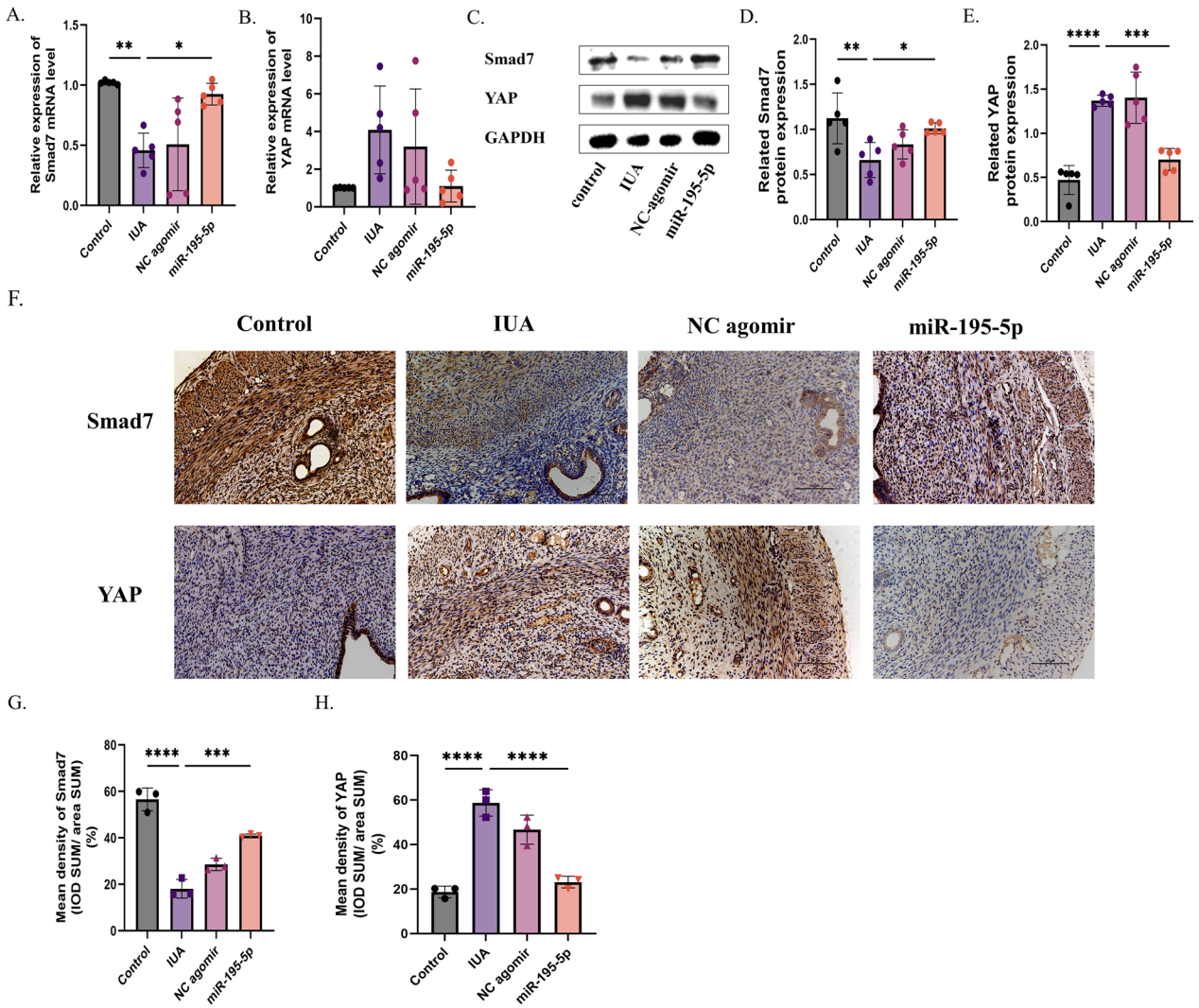

Fig. 4 Agomir-195-5p regulates endometrial fibrosis by inhibiting the YAP-Smad7 pathway. **A**–**E** RT-PCR and Western blot analysis of YAP and Smad7 expression in uterine tissue. **F**–**H** Immunohistochemical analysis of YAP and Smad7 expression in uterine tissue. (ns = not significant, *P < 0.05, **P < 0.01, ****P < 0.001)

mesenchymal marker vimentin and negative for the epithelial marker CK18 (Supplement Fig. 4B).

Decreased expression of miR-195-5p in ESCs after TGF-β treatment

ESCs were treated with different concentrations of TGF-β (0 ng/mL, 5 ng/mL, 10 ng/mL, and 20 ng/mL) and at different times (12 h, 24 h, and 48 h) as shown in Supplement Fig. 4C. The CCK8 assay showed a gradual reduction in ESC activity with an increase in TGF-β concentration and time. Finally, the intervention effect of 10 ng/mL TGF-β was determined. We observed that miR-195-5p expression was downregulated in TGF-β-treated ESCs compared to that in controls (Fig. 5A). Next, we found that miR-195-5p was significantly overexpressed by transfecting miR-195-5p mimics into TGF-β-treated ESCs (Supplement Fig. 4D). (ns = not significant, *P < 0.05, **P < 0.01, ****P < 0.001).

Overexpression of miR-195-5p improves TGF-β-induced myofibroblast transdifferentiation and migration

qRT-PCR results revealed that TGF-β stimulation led to a notable upregulation in the expression of mRNA markers associated with ECM production and myoblast transdifferentiation including collagen I, α-SMA, and Vimentin (Fig. 5B–D). Conversely, the introduction of miR-195-5p resulted in a significant reduction in their expression levels. This contrast was evident in Western blot and immunofluorescence analyses, where TGF-β treatment notably enhanced ECM deposition and the expression of proteins linked to myoblast transdifferentiation, while miR-195-5p overexpression led to a decrease in these protein levels (Fig. 5E–H, Supplement Fig. 3E–J) (ns = not significant, *P < 0.05, **P < 0.01, ****P < 0.001).

Furthermore, scratch and transwell experiments demonstrated that TGF-β treatment effectively promoted the migration of embryonic stem cells (ESCs). Conversely, miR-195-5p overexpression attenuated the migratory capacity of TGF-β-treated ESCs (Fig. 5I–L) (ns = not significant, *P < 0.05, **P < 0.01, ****P < 0.001).

MiR-195-5p regulated TGF-β-induced ECM expression and myofibroblast transdifferentiation in ESCs via the YAP–Smad7 signaling pathway

Firstly, it was confirmed that there exists an interaction between YAP and Smad7, as evidenced by the Co-IP results (Fig. 6A). Subsequent qRT-PCR and Western blot analyses demonstrated that following TGF-β intervention, YAP expression increased while Smad7 mRNA and protein levels decreased. Conversely, overexpression of miR-195-5p led to a reduction in YAP expression and an increase in Smad7 expression (Fig. 6B–F). Furthermore, immunofluorescence staining for YAP and Smad7 co-localization revealed distinct cellular distributions: YAP predominantly localized in the nucleus, whereas Smad7 primarily resided in the cytoplasm. Notably, these localization patterns were consistent with their mRNA and protein expression levels (ns = not significant, *P < 0.05, **P < 0.01, ****P < 0.001).

Further comparison of indicators related to ECM and myofibroblast transdifferentiation among different experimental groups—Smad7 + miR-195-5p overexpression, miR-195-5p overexpression alone, embryonic stem cell (ESC), and TGF-β-treated groups—was conducted. Western blot results illustrated that miR-195-5p overexpression led to a decrease in the expression of related indicators such as α-SMA, type I collagen, and Vimentin (Fig. 6G–I). Conversely, upon blocking the Smad7 pathway, the expressions of α-SMA, type I collagen, and Vimentin in ECM and myofibroblast transdifferentiation indices were increased (Fig. 6J–M). Similarly, we verified these findings on human endometrial stromal cells and obtained consistent results (Supplement Fig. 5) (ns = not significant, *P < 0.05, **P < 0.01, ****P < 0.001).

The effects of miR-195-5P agonist were similar to those of autologous adipose-derived stem cells (ADSCs)

Stem cells are a relatively new therapy for the treatment of IUA. In a previous study, we found autologous ADSCs to improve endometrial fibrosis in mice [8]. Autologous ADSCs were isolated and cultured from the inguinal region of rats and their morphology was mostly polygonal. The adherent cells expanded in vitro and gradually formed spindle-shaped fibroblast-like cells (Fig. 7A). In addition, these cells showed the ability to differentiate into adipocytes, osteoblasts, and chondrocytes in vitro (Fig. 7B). In the third generation, ADSC surface markers were detected using flow cytometry; CD90 and CD29 were positively expressed and CD45 and CD11b/c were negatively expressed, thus demonstrating that we had extracted ADSCs (Fig. 7C).

The homing of DIR-labeled autologous adipose-derived mesenchymal stem cells to the injured uterus was detected using a small animal in vivo imager. The results revealed that within 1 h of in situ injection, fluorescence at the injured site was evident. By 6 h post-injury, the presence of autologous adipose-derived mesenchymal stem cells at the injured site became more pronounced with fluorescence intensifying. Subsequently, fluorescence gradually diminished over 2 days and was nearly absent by day 7 indicating successful homing of autologous adipose-derived mesenchymal stem cells to the injured uterus (Fig. 7D).

Furthermore, ADSCs were administered via local injections in the uterus 7 days after injury. H&E staining showed thickening of the endometrium and

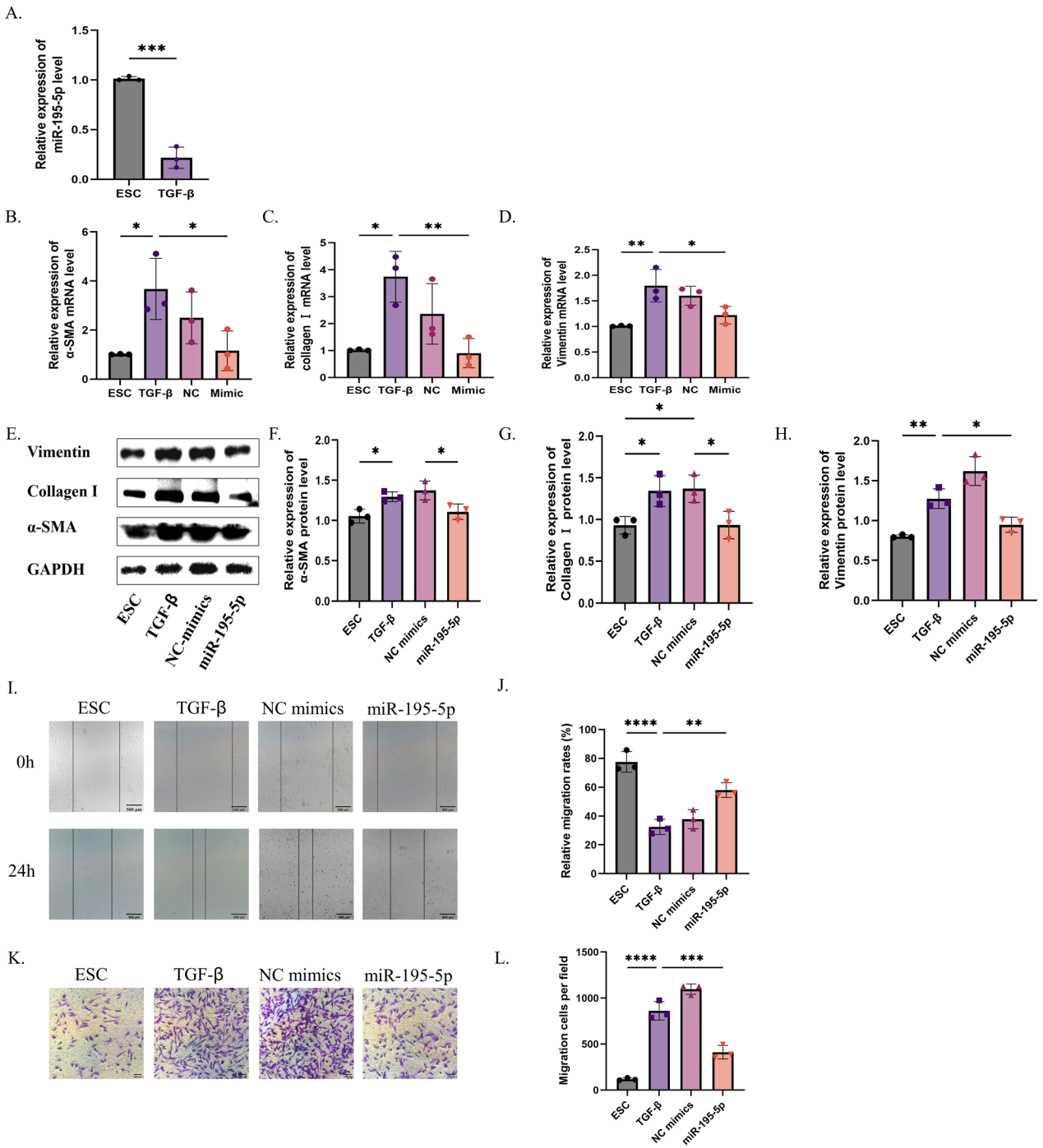

Fig. 5 MiR-195-5p overexpression inhibits migration, ECM deposition, and myofibroblast transdifferentiation of ESCs treated with TGF-β. **A** Verification of miR-195-5p expression in the cell model by RT-PCR. **B**–**H** Expression of ECM-related and myofibroblast transdifferentiation markers (α-SMA, collagen I, and vimentin) analyzed by Western blot and RT-PCR. **I**, **J** Healing ability after miR-195-5p mimic treatment. **K**, **L** Migration ability after miR-195-5p mimic treatment. (ns = not significant, *P < 0.05, **P < 0.01, ****P < 0.001)

enlargement of the glands in the autologous ADSCs and agomir-195-5p-treated groups. Masson's trichrome staining showed decreased fibrotic area after treatment with ADSCs and agomir-195-5p; however, there was no statistical significance between the two treatments, suggesting that the efficacy of agomir-195-5p treatment may achieve the efficacy of autologous ADSCs. In

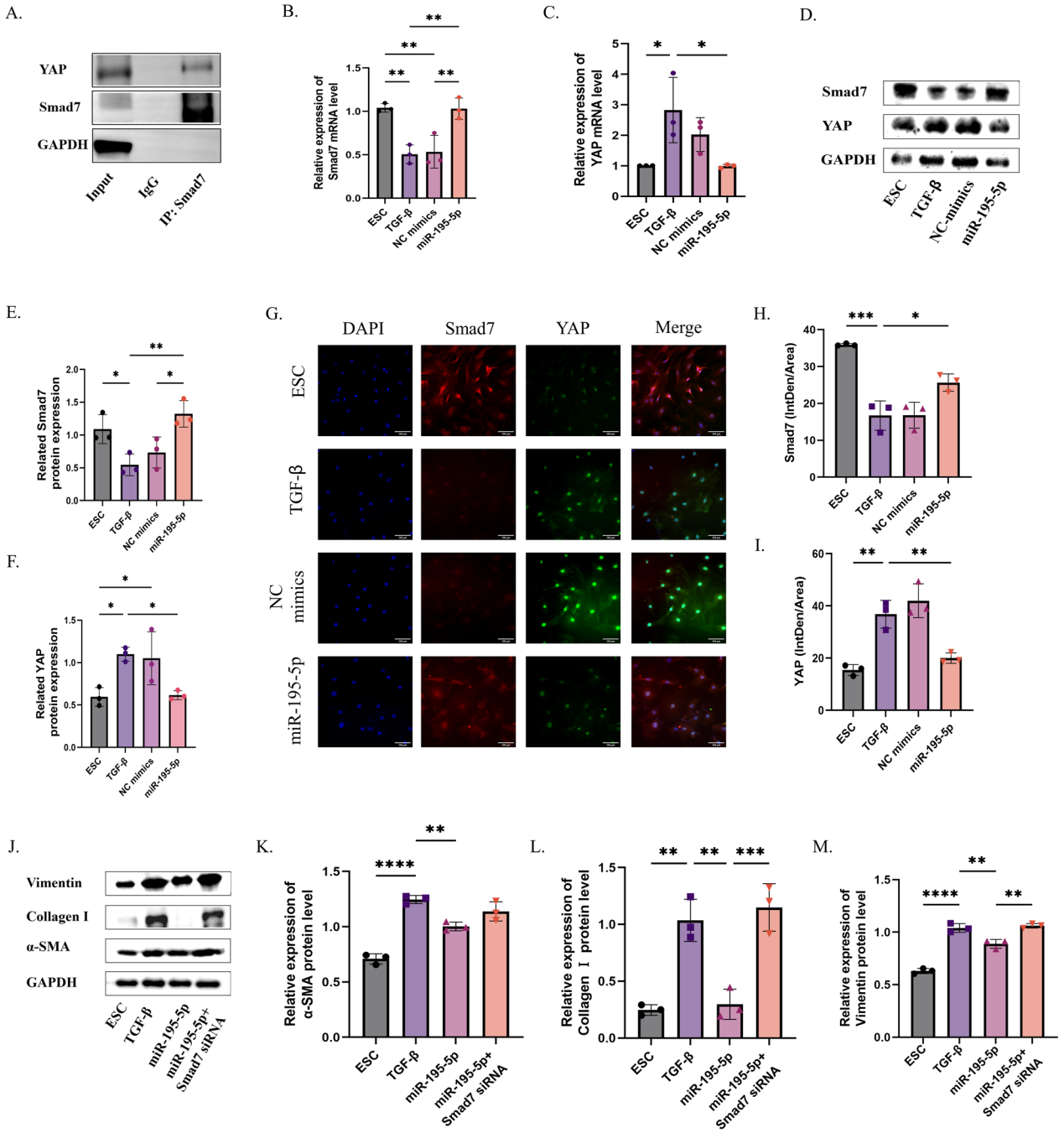

Fig. 6 MiR-195-5p regulates ECM and myofibroblast transdifferentiation of TGF-β-treated ESCs by targeting the YAP-Smad7 signaling pathway. **A** COIP detection of the targeting relationship between YAP and Smad7. **B**–**F** RT-PCR and Western blot analysis of YAP and Smad7 expression in uterine tissue after miR-195-5p mimic treatment. **G**–**I** Immunofluorescence analysis of YAP and Smad7 expression in uterine tissue after miR-195-5p mimic treatment. **J**–**M** Western blot analysis of YAP and Smad7 expression in uterine tissue after miR-195-5p mimic treatment and Smad7 knockdown. (ns = not significant, *P < 0.05, **P < 0.01, ****P < 0.001)

addition, the result suggests that agomir-195-5p can be investigated clinical trials.

In addition, Western blotting was used to compare the ECM and myofibroblast transdifferentiation-related indicators of uterine tissues after treatment. The results showed that the indicators, α-SMA, Collagen I and Vimentin decreased after treatment suggesting that the deposition of ECM and myofibroblast

transdifferentiationmay play a crucial role in the development of endometrial fibrosis.

Discussion

The results of this study showed the following: (1) the relevant indexes of ECM deposition and myofibroblast transdifferentiation changed in the normal and IUA groups; (2) the expression of miR-195-5p in the exosomes of the normal and IUA groups differed, and Smad7 and YAP were downstream target gene of miR-195-5p; (3) after treatment with the miR-195-5p agonist, the endometrium thickened, the glands enlarged, the fibrotic area decreased, and the fertility increased; (4) miR-195-5p regulates ECM deposition and myofibroblast transdifferentiation via the Hippo pathway involving YAP–Smad7 signaling, thereby improving endometrial fibrosis; and (5) autologous stem cell and miR-195-5p agonist treatment improved endometrial fibrosis with comparable efficacy (Fig. 8).

IUA is fibrosis in the uterine cavity. It is the second most common cause of female infertility and seriously affects women's physical and mental health. Current therapeutic strategies have failed to provide satisfactory treatment outcomes for patients with IUA, leaving a great challenge for reproductive science [39]. MiRNAs are highly abundant in utero and are involved in fine-tuning gene regulation during development. In IUA, the expression of various miRNAs is abnormal, leading to alterations in gene expression and function. However, there are few studies on the dynamic changes of miRNA expression in uterine adhesion exosomes. In the present study, we comprehensively analyzed the sequences of miRNAs in uterine tissues of SD rats with IUA and compared them with normal uterine tissues. The results showed that miR-195-5p expression was significantly reduced in the uterine tissues of mice in the IUA group, suggesting that miR-195-5p may be a protective factor in uterine tissues. In addition, bioinformatics analysis revealed that Smad7 was a downstream target of miR-195-5p. qRT-PCR and Western blot analysis results showed that YAP expression increased and Smad7 expression decreased in the injury group; therefore, YAP and Smad7 may be important targets in the pathogenesis and treatment of IUA and the Hippo pathway may be a key pathway in the pathogenesis and treatment of IUA.

In recent years, research has shown that TGF-β overexpression leads to excessive metabolic disorders and dysfunction, which subsequently promotes myofibroblast transdifferentiation and excessive deposition of the ECM, inducing immune dysfunction, fibrosis, and cancer [40]. Studies have shown that myofibroblast transdifferentiation and ECM deposition are closely related to various signaling pathways. AMPK signaling can inhibit myofibroblast differentiation by targeting pathways such as TGF-β, NF-κB, STAT3, and YAP/TAZ. By inhibiting myofibroblast differentiation, AMPK signaling appears to alleviate age-related tissue fibrosis and degeneration [24]. What's more, Wang et al. [41] found that the interaction between JAK1/STAT3 and TGF-β regulates the transdifferentiation and fibrosis of myofibroblasts, and suggested the potential of a new method for the treatment of pulmonary fibrosis. Our studies have also shown that IUA is closely associated with myofibroblast transdifferentiation and ECM deposition [42]. We found increased expression of ECM and myofibroblast transdifferentiation-related indicators, α-SMA, Collagen I, and Vimentin in the normal and IUA groups. These results indicate that the development of IUA was accompanied by ECM deposition and myofibroblast transdifferentiation.

Due to the high recurrence rate of severe intrauterine adhesions, researchers have been exploring treatment methods to improve the prognosis of this condition in recent years. Luo et al. [43]. found through meta-analysis that hyaluronic acid can safely and effectively reduce the occurrence of intrauterine adhesions and may improve fertility outcomes. In addition, Ding et al. [44]. found that inserting a balloon or placing an intrauterine device for one to two months can effectively reduce the risk of adhesion recurrence and restore the shape of the uterine cavity. Although the therapeutic effect of balloon was better than that of intrauterine device, no significant difference was observed in the intrauterine device group at 1 month and 2 months. However, the current treatment method is still very high for the recurrence rate of severe intrauterine adhesions, and the targeting is low. Therefore, we explore new treatment methods by finding differential miRNAs in

(See figure on next page.)

Fig. 7 Comparison of the efficacy of autologous adipose-derived mesenchymal stem cells (ADSCs) and miR-195-5p. **A** Microscopy assessment of autologous ADSCs morphology from passage 0 (P0) to P3, showing their adhesiveness and fibroblastoid shape. **B** Osteogenic, adipogenic, and chondrogenic differentiation of ADSCs. **C** Flow cytometry detection of ADSC surface markers CD29, CD90, CD45, and CD11b/c. **D** In vivo imaging of ADSC homing in intrauterine adhesions. **E**–**G** H&E staining of uterine morphology with statistical analysis of endometrial thickness and gland number. **H**, **I** Assessment of fibrotic area in the endometrium using Image Pro Plus 6.0 and Masson staining. **J**–**M** Western blot analysis of ECM and myofibroblast transdifferentiation markers (α-SMA, collagen I, and vimentin) in IUA

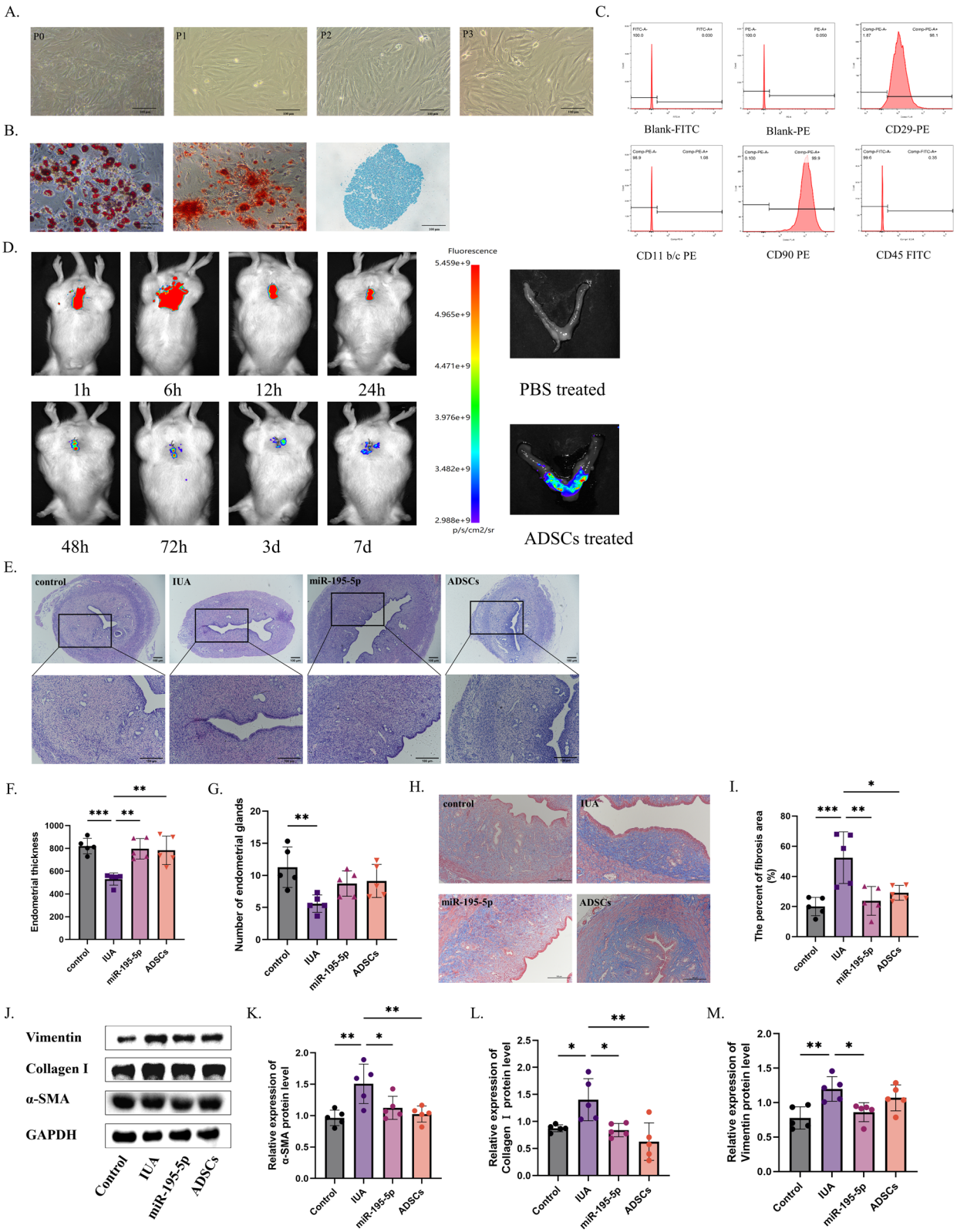

Fig. 7 (See legend on previous page.)

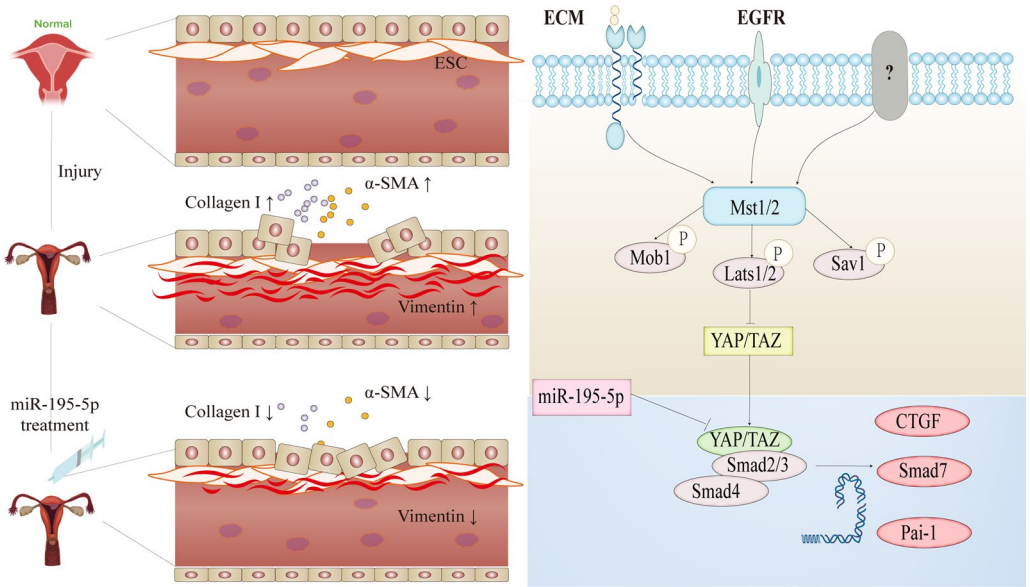

Fig. 8 Summary chart. This study begins with models of normal and intrauterine adhesions. To investigate the fibrosis mechanism, we identified differential miR-195-5p through tissue exosome sequencing and verified our findings across cell, tissue, animal, and human levels. Treatment with agomir-195-5p increased Smad7 by inhibiting YAP in the Hippo pathway, reducing ECM deposition and reversing myofibroblast transdifferentiation. This led to the repair of endometrial fibrosis, resulting in a thicker endometrium and increased gland number

uterine tissue exosomes of intrauterine adhesions and further exploring their target genes, hoping to improve the poor prognosis of intrauterine adhesions.

To further demonstrate that the decrease in miR-195-5p observed in our tissue exosomes is a pathogenic factor in intrauterine adhesions (IUA), we utilized miR-195-5p agonists in both animal and cell models, with corresponding control groups. The results showed that after treatment with miR-195-5p agonists, the endometrium thickened, the number of glands increased, the fibrotic area reduced, and indicators of ECM deposition and myofibroblast transdifferentiation improved. This suggests that the reduction of miR-195-5p is a significant cause of IUA. The miR-195-5p agonists ameliorated endometrial fibrosis by regulating ECM deposition and myofibroblast transdifferentiation.

To explore how miR-195-5p agonists exert their effects, we investigated the downstream target gene of miR-195-5p, Smad7. Using dual luciferase labeling, we confirmed that Smad7 is indeed a target gene of miR-195-5p. Previous studies have identified Smad7 as a target of miR-195-5p. For example, Ding et al. [45] found that downregulation of miR-195-5p inhibited endothelial-mesenchymal transition and myocardial fibrosis in diabetic cardiomyopathy by targeting Smad7 and inhibiting the TGF-β1-Smad-Snail pathway. Similarly, Lin et al. [46] discovered that miR-195-5p promoted the Wnt/β-catenin pathway by targeting Smad7, thereby enhancing the osteogenic differentiation of VSMCs. These findings support Smad7 as a target gene of miR-195-5p.

In order to further explore the role of Smad7 in the Hippo pathway in IUA, we further studied the important key gene YAP in the Hippo pathway. Our experiments revealed that YAP increased and Smad7 decreased after injury, whereas YAP decreased and Smad7 increased after treatment with miR-195-5p agonists. By inhibiting Smad7 expression following miR-195-5p treatment, the therapeutic effect through the Hippo pathway was nullified, indicating that the miR-195-5p agonist operates via the YAP–Smad7 axis in the Hippo pathway. This mechanism reduced ECM deposition and reversed myofibroblast transdifferentiation, thereby improving endometrial fibrosis. The same therapeutic effects were confirmed in human cells.

Compared with current treatments for intrauterine adhesions, miR-195-5p agonist therapy offers advantages such as no immune rejection and easier obtainability. Additionally, miR-195-5p provides a more targeted approach, potentially enabling more precise clinical treatment of intrauterine adhesions. However, there remain many unknowns regarding the clinical application of miR-195-5p agonists, and further research is needed to evaluate dosage and patient prognosis during the translational process.

Stem cell therapy holds great promise for the repair and regeneration of injured tissues. In endometrial regeneration, stem cell therapy is performed by intravenous or

intrauterine injection [47]. In our previous experiments, we verified the efficacy of autologous ADSCs on IUA in mice [8]. To further elucidate the therapeutic effect of miR-195-5p agonist on IUA, we compared the efficacy of the miR-195-5p agonist and autologous ADSCs in the treatment of IUA. Experimentally, we found that endometrial thickening, glandular increase, and reduction of fibrotic area were observed after treatment. The efficacy of treatment with the miR-195-5p agonist was comparable to that of the ADSCs, offering the possibility for the clinical translation of miR-195-5p.

Conclusion

In conclusion, to the best of our knowledge, this is the first study to identify the differential expression of miR-195-5p from tissue exosomes and verify the effect of miR-195-5p agonists on IUA from tissue and cell models from animals and humans, as well as the role of the miR-195-5p agonist in ECM deposition and myofibroblast transdifferentiation. Validation of Smad7, a miR-195-5p-enriched target gene, ultimately revealed that miR-195-5p promotes ECM deposition, reverses myofibroblast transdifferentiation, and ameliorates endometrial fibrosis via YAP–Smad7.

However, due to the differences in tissue exosomes, we did not directly use them for treatment. Normal uterine tissue exosomes may contain more IUA therapeutic factors. Unlike stem cell therapy, the use of exosomes does not cause problems such as immune rejection, and can be more effectively applied in clinical practice. Besides, the application of miR-195-5p agonists in clinical practice may also have the possibility of off-target, and the clinical application of exosomes in intrauterine adhesions is less, and its safety and prognosis are still unknown. In the future, we will continue to study the efficacy of uterine tissue exosomes on IUAs to enhance the therapeutic effect, and gradually apply exosomes to clinical treatment of intrauterine adhesions. What's more, due to the challenges of obtaining uterine tissue exosomes for clinical application, we will explore the use of exosomes with nanoenzyme bioscaffolds to prolong their retention time in vivo.

Additionally, during the animal mating experiments, we did not evaluate the health status of the young mice due to limited experimental conditions. In subsequent experiments, we will further observe the live birth rate of offspring and use ultrasound to examine the uteri of female SD rats. Furthermore, we will focus on clinical translation by comparing the efficacy of miR-195-5p and autologous adipose-derived mesenchymal stem cells in patients, and evaluating their safety, long-term efficacy, and prognosis.

In addition, from the mechanism point of view, YAP is the core process in the Hippo pathway. It is a transcriptional co-activator that plays a mechanical transduction role in the cell. It can respond to a variety of mechanical signals, such as fluid shear stress, extracellular matrix stiffness, etc. Due to the limited experimental conditions, the role of YAP in regulating the stiffness of extracellular matrix in intrauterine adhesions will be further explored in the future.

Abbreviations

IUA	Intrauterine adhesion
ADSCs	Adipose-derived stem cells
IHC	Immunohistochemical
qRT-PCR	Quantitative real-time polymerase chain reaction
H&E	Hematoxylin and eosin
PBS	Phosphate-buffered
FBS	Fetal bovine serum
α-SMA	α-Smooth muscle actin
MET	Mesenchymal–epithelial transition
TGF-β	Transforming growth factor-β
FSP-1	Fibroblast specific protein 1
EV	Exosome
CTGF	Connective tissue growth factor
ROCK1	Rho associated coiled coil containing protein kinase 1
TAZ	Tafazzin
YAP	Yes-associated protein 1
TEAD	Transcriptional enhanced associate domain
ECM	Extracellular matrix
SD	Sprague Dawley
DMEM	Dulbecco's modified Eagle's medium
STAR	Steroidogenic acute regulatory
BCA	Bicinchoninic acid
GAPDH	Glyceraldehyde-3-phosphate dehydrogenase
smad7	Drosophila mothers against decapentaplegic 7
DAB	Diaminobenzidine
MOD	Mean optical density
ESC	Endometrial stromal cells
DMEM/F12	Dulbecco's modified Eagle's medium/nutrient mixture F-12
CCK-8	Cell Counting Kit-8
ANOVA	One-way analysis of variance
DLS	Dynamic Light Scattering
TEM	Transmission electron microscope

Supplementary Information

The online version contains supplementary material available at https://doi.org/10.1186/s12967-024-05871-8.

Supplementary Material 1: Figure 1. Intrauterine adhesion (IUA) causes ECM deposition and myofibroblast transdifferentiation. (A) Normal estrous cycle in SD rats. (B) H&E staining of uterine morphology. (C-D) Statistical analysis of endometrial thickness and gland number. (E) Assessment of fibrosis extent using Masson staining. (F) Fibrotic area analysis with Image Pro Plus 6.0. (G-I) Western blot and RT-PCR analysis of ECM deposition and myofibroblast transdifferentiation markers (α-SMA, collagen I, vimentin) in IUA (ns = not significant, *P < 0.05, **P < 0.01, ****P < 0.001).

Supplementary Material 2: Figure 2. Identification of uterine tissue exosomes. (A) DLS measurement of exosome diameter. (B) Electron microscopy of exosome morphology. (C) Flow cytometry analysis of exosome surface markers CD9 and CD63.

Supplementary Material 3: Figure 3 (A-B) GO and KEGG enrichment analyses of miR-195-5p target genes. (C-D) Heat map and volcano plot showing differential genes in GSE224093. (E-F) PPI network constructed by STRING and Cytoscape to determine miR-195-5p target genes and related pathways.

Supplementary Material 4: Figure 4. (A) Extracted ESCs from SD rats showing fusiform growth. (B) Identification of extracted ESCs by immunofluorescence (IF). (C) CCK8 assay to detect cell proliferation after TGF-β treatment. (D) Expression level of miR-195-5p after miR-195-5p mimic treatment. (E-J) Expression of ECM and myofibroblast transdifferentiation markers (α-SMA, collagen I, vimentin) in IUA analyzed by IF (ns = not significant, *P < 0.05, **P < 0.01, ****P < 0.001).

Supplementary Material 5: Figure 5. MiR-195-5p mimic improves epithelial-mesenchymal transition of human endometrial stromal cells (hESCs) via YAP-Smad7. (A) Fusiform growth of extracted hESCs. (B) Identification of extracted hESCs by IF. (C) Verification of miR-195-5p expression in hESCs by RT-PCR. (D-G) Western blot analysis of ECM and myofibroblast transdifferentiation markers (α-SMA, collagen I, vimentin) in IUA. (H-J) Western blot analysis of YAP and Smad7 expression in hESCs after miR-195-5p mimic treatment (ns = not significant, *P < 0.05, **P < 0.01, ****P < 0.001).

Acknowledgements
We are thankful to The Second Affiliated Hospital of Fujian Medical University for providing infrastructure facilities. Additionally, we would like to thank Editage (www.editage.cn) for English language editing.

Author contributions
SL and QS designed the study methodology. JC, QH, and WC collected the data and JW, LZ, HY, and YS analyzed the results. JC drafted the article. All authors reviewed and revised the work, and all authors reviewed the final article and approved it for submission.

Funding
This work was supported by the Science and Technology Bureau of Quanzhou (Grant number 2020CT003) and Fujian Provincial Health Commission youth fund project (Grant number 2022QNA067), Fujian Provincial Health Commission science and technology (Grant number 2020CXB027), Science and Technology Bureau of Quanzhou (Grant number 2020N031s), Joint funds for the innovation of science and technology, Fujian province(Grant number: 2023Y9254).

Availability of data and materials
The data supporting the results of this study can be obtained from the corresponding authors under reasonable requirements.

Declarations

Ethics approval and consent to participate
This study involves the collection of human endometrium and animal as part of the project titled 'Study on the mechanism of miR-195-5p improving the epithelial-mesenchymal transformation of endometrial adhesion through YAP-SMAD7, which was approved by the Second Affiliated Hospital of Fujian Medical University Animal Care Committee (Approval No. and Date: 2023-179, May 18, 2023).

Consent for publication
Not applicable.

Competing interests
The authors declare that they have no competing interests.

Author details
[1]Department of Gynaecology and Obstetrics, The Second Affiliated Hospital of Fujian Medical University, Quanzhou 362000, Fujian Province, China. [2]Department of Reproductive Medicine, The Second Affiliated Hospital of Fujian Medical University, Quanzhou 362000, Fujian Province, China. [3]Group of Neuroendocrinology, Garvan Institute of Medical Research, 384 Victoria St, Sydney 999029, Australia. [4]St Vincent's Clinical School, Faculty of Medicine, UNSW Sydney, Sydney 999029, Australia. [5]Centre of Neurological and Metabolic Research, The Second Affiliated Hospital of Fujian Medical University, Quanzhou 362000, Fujian Province, China.

Received: 29 April 2024 Accepted: 9 November 2024
Published online: 21 November 2024

References

1. Song YT, Liu PC, Tan J, Zou CY, Li QJ, Li-Ling J, Xie HQ. Stem cell-based therapy for ameliorating intrauterine adhesion and endometrium injury. Stem Cell Res Ther. 2021;12:556.
2. Kou L, Jiang X, Xiao S, Zhao YZ, Yao Q, Chen R. Therapeutic options and drug delivery strategies for the prevention of intrauterine adhesions. J Control Release. 2020;318:25–37.
3. Deans R, Abbott J. Review of intrauterine adhesions. J Minim Invasive Gynecol. 2010;17:555–69.
4. Salma U, Xue M, Md Sayed AS, Xu D. Efficacy of intrauterine device in the treatment of intrauterine adhesions. Biomed Res Int. 2014;2014:589296.
5. Cai Y, Wu F, Yu Y, Liu Y, Shao C, Gu H, Li M, Zhao Y. Porous scaffolds from droplet microfluidics for prevention of intrauterine adhesion. Acta Biomater. 2019;84:222–30.
6. Li Y, Guo F, Hao Y, Gupta SK, Hu J, Wang Y, Wang N, Zhao Y, Guo M. Helical nanofiber yarn enabling highly stretchable engineered microtissue. Proc Natl Acad Sci USA. 2019;116:9245–50.
7. Xin L, Wei C, Tong X, Dai Y, Huang D, Chen J, Ma L, Zhang S. In situ delivery of apoptotic bodies derived from mesenchymal stem cells via a hyaluronic acid hydrogel: a therapy for intrauterine adhesions. Bioact Mater. 2022;12:107–19.
8. Zhao YX, Chen SR, Huang QY, Chen WC, Xia T, Shi YC, Gao HZ, Shi QY, Lin S. Repair abilities of mouse autologous adipose-derived stem cells and ShakeGel3D complex local injection with intrauterine adhesion by BMP7-Smad5 signaling pathway activation. Stem Cell Res Ther. 2021;12:191.
9. Chen JM, Huang QY, Chen WH, Lin S, Shi QY. Clinical evaluation of autologous and allogeneic stem cell therapy for intrauterine adhesions: a systematic review and meta-analysis. Front Immunol. 2022;13: 899666.
10. Choi DS, Kim DK, Kim YK, Gho YS. Proteomics of extracellular vesicles: exosomes and ectosomes. Mass Spectrom Rev. 2015;34:474–90.
11. Al-Nedawi K, Meehan B, Micallef J, Lhotak V, May L, Guha A, Rak J. Intercellular transfer of the oncogenic receptor EGFRvIII by microvesicles derived from tumour cells. Nat Cell Biol. 2008;10:619–24.
12. Antonyak MA, Li B, Boroughs LK, Johnson JL, Druso JE, Bryant KL, Holowka DA, Cerione RA. Cancer cell-derived microvesicles induce transformation by transferring tissue transglutaminase and fibronectin to recipient cells. Proc Natl Acad Sci USA. 2011;108:4852–7.
13. Ning J, Zhang H, Yang H. MicroRNA-326 inhibits endometrial fibrosis by regulating TGF-beta1/Smad3 pathway in intrauterine adhesions. Mol Med Rep. 2018;18:2286–92.
14. Li J, Du S, Sheng X, Liu J, Cen B, Huang F, He Y. MicroRNA-29b inhibits endometrial fibrosis by regulating the Sp1-TGF-beta1/Smad-CTGF axis in a rat model. Reprod Sci. 2016;23:386–94.
15. Wu D, Lu P, Mi X, Miao J. Exosomal miR-214 from endometrial stromal cells inhibits endometriosis fibrosis. Mol Hum Reprod. 2018;24:357–65.
16. Xu Q, Duan H, Gan L, Liu X, Chen F, Shen X, Tang YQ, Wang S. MicroRNA-1291 promotes endometrial fibrosis by regulating the ArhGAP29-RhoA/ROCK1 signaling pathway in a murine model. Mol Med Rep. 2017;16:4501–10.
17. Ai Y, Chen M, Liu J, Ren L, Yan X, Feng Y. lncRNA TUG1 promotes endometrial fibrosis and inflammation by sponging miR-590-5p to regulate Fasl in intrauterine adhesions. Int Immunopharmacol. 2020;86: 106703.
18. Zhao G, Li R, Cao Y, Song M, Jiang P, Wu Q, Zhou Z, Zhu H, Wang H, Dai C, Liu D, Yao S, Lv H, Wang L, Dai J, Zhou Y, Hu Y. DeltaNp63alpha-induced DUSP4/GSK3beta/SNAI1 pathway in epithelial cells drives endometrial fibrosis. Cell Death Dis. 2020;11:449.
19. Zhu H, Pan Y, Jiang Y, Li J, Zhang Y, Zhang S. Activation of the Hippo/TAZ pathway is required for menstrual stem cells to suppress myofibroblast and inhibit transforming growth factor beta signaling in human endometrial stromal cells. Hum Reprod. 2019;34:635–45.
20. Lv H, Nan Z, Jiang P, Wang Z, Song M, Ding H, Liu D, Zhao G, Zheng Y, Hu Y. Vascular endothelial growth factor 165 inhibits pro-fibrotic differentiation of stromal cells via the DLL4/Notch4/smad7 pathway. Cell Death Dis. 2019;10:681.

21. Abreu JG, Ketpura NI, Reversade B, De Robertis EM. Connective-tissue growth factor (CTGF) modulates cell signalling by BMP and TGF-beta. Nat Cell Biol. 2002;4:599–604.
22. Sonnylal S, Shi-Wen X, Leoni P, Naff K, Van Pelt CS, Nakamura H, Leask A, Abraham D, Bou-Gharios G, de Crombrugghe B. Selective expression of connective tissue growth factor in fibroblasts in vivo promotes systemic tissue fibrosis. Arthritis Rheum. 2010;62:1523–32.
23. Chen Y, Bai X, Chen J, Huang M, Hong Q, Ouyang Q, Sun X, Zhang Y, Liu J, Wang X, Wu L, Chen X. Pyruvate kinase M2 regulates kidney fibrosis through pericyte glycolysis during the progression from acute kidney injury to chronic kidney disease. Cell Prolif. 2024;57: e13548.
24. Salminen A. AMPK signaling inhibits the differentiation of myofibroblasts: impact on age-related tissue fibrosis and degeneration. Biogerontology. 2024;25:83–106.
25. Meng S, Wei Q, Chen S, Liu X, Cui S, Huang Q, Chu Z, Ma K, Zhang W, Hu W, Li S, Wang Z, Tian L, Zhao Z, Li H, Fu X, Zhang C. MiR-141-3p-functionalized exosomes loaded in dissolvable microneedle arrays for hypertrophic scar treatment. Small. 2024;20: e2305374.
26. Zhu Y, Hu J, Yu T, Ren Y, Hu L. High molecular weight hyaluronic acid inhibits fibrosis of endometrium. Med Sci Monit. 2016;22:3438–45.
27. Xue X, Chen Q, Zhao G, Zhao JY, Duan Z, Zheng PS. The overexpression of TGF-beta and CCN2 in intrauterine adhesions involves the NF-kappaB signaling pathway. PLoS ONE. 2015;10: e0146159.
28. Wang X, Ma N, Sun Q, Huang C, Liu Y, Luo X. Elevated NF-kappaB signaling in Asherman syndrome patients and animal models. Oncotarget. 2017;8:15399–406.
29. Placek K, Schultze JL, Aschenbrenner AC. Epigenetic reprogramming of immune cells in injury, repair, and resolution. J Clin Invest. 2019;129:2994–3005.
30. Jorgenson AJ, Choi KM, Sicard D, Smith KM, Hiemer SE, Varelas X, Tschumperlin DJ. TAZ activation drives fibroblast spheroid growth, expression of profibrotic paracrine signals, and context-dependent ECM gene expression. Am J Physiol Cell Physiol. 2017;312:C277–85.
31. Speight P, Nakano H, Kelley TJ, Hinz B, Kapus A. Differential topical susceptibility to TGFbeta in intact and injured regions of the epithelium: key role in myofibroblast transition. Mol Biol Cell. 2013;24:3326–36.
32. Lei QY, Zhang H, Zhao B, Zha ZY, Bai F, Pei XH, Zhao S, Xiong Y, Guan KL. TAZ promotes cell proliferation and epithelial–mesenchymal transition and is inhibited by the hippo pathway. Mol Cell Biol. 2008;28:2426–36.
33. Brewer CM, Nelson BR, Wakenight P, Collins SJ, Okamura DM, Dong XR, Mahoney Jr WM, McKenna A, Shendure J, Timms A, Millen KJ, Majesky MW. Adaptations in Hippo-Yap signaling and myofibroblast fate underlie scar-free ear appendage wound healing in spiny mice. Dev Cell. 2021;56:2722–27406.
34. Shen H, Huang X, Zhao Y, Wu D, Xue K, Yao J, Wang Y, Tang N, Qiu Y. The Hippo pathway links adipocyte plasticity to adipose tissue fibrosis. Nat Commun. 2022;13:6030.
35. Wang Q, Xu Z, An Q, Jiang D, Wang L, Liang B, Li Z. TAZ promotes epithelial to mesenchymal transition via the upregulation of connective tissue growth factor expression in neuroblastoma cells. Mol Med Rep. 2015;11:982–8.
36. Shen X, Cheng S, Peng Y, Song H, Li H. Attenuation of early liver fibrosis by herbal compound "Diwu Yanggan" through modulating the balance between epithelial-to-mesenchymal transition and mesenchymal-to-epithelial transition. BMC Complement Altern Med. 2014;14:418.
37. Song Y, Fu J, Zhou M, Xiao L, Feng X, Chen H, Huang W. Activated hippo/yes-associated protein pathway promotes cell proliferation and anti-apoptosis in endometrial stromal cells of endometriosis. J Clin Endocrinol Metab. 2016;101:1552–61.
38. Zhang S, Li P, Yuan Z, Tan J. Platelet-rich plasma improves therapeutic effects of menstrual blood-derived stromal cells in rat model of intrauterine adhesion. Stem Cell Res Ther. 2019;10:61.
39. Feng L, Wang L, Ma Y, Duan W, Martin-Saldana S, Zhu Y, Zhang X, Zhu B, Li C, Hu S, Bao M, Wang T, Zhu Y, Yang F, Bu Y. Engineering self-healing adhesive hydrogels with antioxidant properties for intrauterine adhesion prevention. Bioact Mater. 2023;27:82–97.
40. Peng D, Fu M, Wang M, Wei Y, Wei X. Targeting TGF-beta signal transduction for fibrosis and cancer therapy. Mol Cancer. 2022;21:104.
41. Wang F, Wang S, Zhang C, Tian X, Zhou Y, Xuan W, Matteson EL, Luo F, Tschumperlin D, Vassallo R. Noncanonical JAK1/STAT3 interactions with TGF-beta modulate myofibroblast transdifferentiation and fibrosis. Am J Physiol Lung Cell Mol Physiol. 2022;323:L698–714.
42. Chen Y, Sun D, Shang D, Jiang Z, Miao P, Gao J. miR-223-3p alleviates TGF-beta-induced epithelial–mesenchymal transition and extracellular matrix deposition by targeting SP3 in endometrial epithelial cells. Open Med (Wars). 2022;17:518–26.
43. Luo Y, Sun Y, Huang B, Chen J, Xu B, Li H. Effects and safety of hyaluronic acid gel on intrauterine adhesion and fertility after intrauterine surgery: a systematic review and meta-analysis with trial sequential analysis of randomized controlled trials. Am J Obstet Gynecol. 2024;231(36–50):35.
44. Ding H, Zhang H, Qiao R, Sun N, Ji Y, Pang W, Li W, Zhang Q. Comparing the efficacy and pregnancy outcome of intrauterine balloon and intrauterine contraceptive device in the prevention of adhesion reformation after hysteroscopic adhesiolysis in infertile women: a prospective, randomized, controlled trial study. Reprod Biol Endocrinol. 2024;22:49.
45. Ding H, Yao J, Xie H, Wang C, Chen J, Wei K, Ji Y, Liu L. MicroRNA-195-5p downregulation inhibits endothelial mesenchymal transition and myocardial fibrosis in diabetic cardiomyopathy by targeting Smad7 and inhibiting transforming growth factor beta 1-smads-snail pathway. Front Physiol. 2021;12: 709123.
46. Lin W, Hou L, Tang J, Huang A, Jia Z. Mir-195-5p targets Smad7 regulation of the Wnt/beta-catenin pathway to promote osteogenic differentiation of vascular smooth muscle cells. BMC Cardiovasc Disord. 2024;24:221.
47. Azizi R, Aghebati-Maleki L, Nouri M, Marofi F, Negargar S, Yousefi M. Stem cell therapy in Asherman syndrome and thin endometrium: stem cell-based therapy. Biomed Pharmacother. 2018;102:333–43.

Publisher's Note